THE JOURNAL OF BIOLOGICAL CHEMISTRY VOL. 283, NO. 34, pp. 23440–23449, August 22, 2008

Par-3-mediated Junctional Localization of the Lipid Phosphatase PTEN Is Required for Cell Polarity Establishment*[S]

Received for publication, March 31, 2008, and in revised form, May 28, 2008 Published, JBC Papers in Press, June 10, 2008, DOI 10.1074/jbc.M802482200

Wei Feng[1], **Hao Wu**[1], **Ling-Nga Chan, and Mingjie Zhang**[2]

From the Department of Biochemistry, Molecular Neuroscience Center, The Hong Kong University of Science and Technology, Clear Water Bay, Kowloon, Hong Kong

PDZ domain-containing scaffold protein Par-3 is the central organizer of the evolutionarily conserved cell polarity-regulatory Par-3·Par-6·atypical protein kinase C complex. The PDZ domains of Par-3 have also been implicated as potential phosphoinositide signaling integrators, since its second PDZ domain binds to phosphoinositides, and the third PDZ interacts with phosphoinositide phosphatase PTEN. However, the molecular basis of Par-3/PTEN interaction is still poorly understood. Additionally, it is not known whether the regulatory function of PTEN in cell polarity is specifically mediated by its interaction with Par-3. The structures of Par-3 PDZ3 in both its free and PTEN tail peptide-bound forms determined in this work reveal that Par-3 PDZ3 binds to PTEN with two discrete binding sites: a canonical PDZ-ligand interaction site and a distal, opposite charge-charge interaction site. This distinct target recognition mechanism confers the interaction specificity of the Par-3·PTEN complex. We show that the Par-3 PDZ3-PTEN binding is required for the enrichment of PTEN at the junctional membranes of Madin-Darby canine kidney cells. Finally, we demonstrate that the junctional membrane-localized PTEN is specifically required for the polarization of Madin-Darby canine kidney cells. These results, together with earlier data, firmly establish that Par-3 functions as a scaffold in integrating phosphoinositide signaling events during cellular polarization.

The polarization of cells is a fundamental process required for the differentiation, proliferation, and morphogenesis of both unicellular and multicellular organisms (1–5). Several common sets of proteins, initially identified through genetic screenings, are known to be essential for the establishment and maintenance of cell polarity (for reviews, see Refs. 6–11). Par (partitioning-defective) proteins, originally discovered in studies of embryonic asymmetric cell division in the *Caenorhabditis elegans* zygote, are one set of these obligatory cell polarity-controlling proteins (7, 12–15). Among the Par proteins, Par-3 and Par-6 are PDZ domain-containing scaffold proteins, and they often localize and function together in places such as the anterior of the *C. elegans* zygote during asymmetric embryonic cell division (16, 17). Both Par-3 and Par-6 can directly interact with atypical protein kinase C (aPKC).[3] This evolutionarily conserved Par-3·Par-6·aPKC complex is absolutely required for the establishment and maintenance of the polarity of essentially all multicellular eukaryotic cells (18–20).

Par-3 contains an N-terminal domain followed by three PDZ domains and an extended C terminus. In addition to binding directly to both Par-6 and aPKC, the N-terminal domain of Par-3 can self-oligomerize, thereby promoting the formation of large assemblies of the Par-3·Par-6·aPKC macromolecular complexes (18, 19, 21). Thus, Par-3 is viewed as the central organizer of the Par-3·Par-6·aPKC assembly. Among the three PDZ domains of Par-3, the first PDZ domain was reported to bind to a number of membrane proteins, such as the neurotrophin receptor p75NTR (22), the junctional adhesion molecule (23), and the cell-cell adhesion molecule nectin (24). Unexpectedly, the second PDZ domain of Par-3 was shown to bind directly to phosphoinositide lipid-containing membranes with high affinity, and this PDZ-lipid membrane interaction is critical for the function of Par-3 in the polarization of MDCK cells (25). An intriguing and potentially important finding was that the third PDZ domain of Par-3 can directly interact with the C terminus of PTEN, a phosphatidylinositol 3,4,5-trisphosphate-specific phosphatase (25–27). Since polarized distribution of phosphoinositide lipids, especially phosphatidylinositol 3,4,5-trisphosphate and PI(4,5)P2, are known to be critical for cell polarity (28–31), it was proposed that Par-3 could function as a potential "gatekeeper" to maintain the phosphoinositide concentration gradient in polarized cells (25). However, this bold speculation needs support from further experimental data. A key line of experimental data that could support the proposed model would be to elucidate the mechanism of the Par-3·PTEN complex formation and to demonstrate that the portion of PTEN localized at junctional membranes by Par-3 PDZ3 binding is specifically required for cell polarity.

* This work was supported by Research Grants Council of Hong Kong Grants HKUST6419/05M, 6442/06M, 663407, AoE/B-15/01-II, and CA07/08.SC01 (to M. Z.). The NMR spectrometer used in this work was purchased with funds donated to the Biotechnology Research Institute by the Hong Kong Jockey Club. The costs of publication of this article were defrayed in part by the payment of page charges. This article must therefore be hereby marked "*advertisement*" in accordance with 18 U.S.C. Section 1734 solely to indicate this fact.

[S] The on-line version of this article (available at http://www.jbc.org) contains supplemental Figs. 1–5.

The atomic coordinates and structure factors (code 2k1z and 2k20) have been deposited in the Protein Data Bank, Research Collaboratory for Structural Bioinformatics, Rutgers University, New Brunswick, NJ (http://www.rcsb.org/).

[1] Both authors contributed equally to this work.

[2] Recipient of the Croucher Foundation Senior Research Fellow Award. To whom correspondence should be addressed. Tel.: 852-2358-8709; Fax: 852-2358-1552; E-mail: mzhang@ust.hk.

[3] The abbreviations used are: aPKC, atypical protein kinase C; MDCK, Madin-Darby canine kidney; PI(4,5)P2, phosphatidylinositol 4,5-bisphosphate; GST, glutathione *S*-transferase; NOE, nuclear Overhauser effect; NOESY, NOE spectroscopy; GFP, green fluorescent protein; PH, pleckstrin homology; HCM, high calcium medium; shRNA, short hairpin RNA.

Here, we have determined the solution structure of Par-3 PDZ3 alone and in complex with the PTEN C-terminal tail peptide by NMR spectroscopy. We discovered that the interaction between Par-3 PDZ3 and the PTEN tail peptide is distinct from all known canonical PDZ-target complexes. We further showed that the junctional membrane localization of PTEN depends on this specific Par-3 PDZ3-PTEN tail peptide interaction. Finally, our data demonstrate that Par-3 PDZ3-mediated PTEN localization to the membrane junctions is essential for the polarization of MDCK cells.

EXPERIMENTAL PROCEDURES

Protein Purification and Antibodies—The coding sequence for Par-3 PDZ3 (residues 579–704) was PCR-amplified from the full-length rat *Par-3* (ASIP) and cloned into a modified pET32a vector. Rat PTEN construct was described in our earlier work (25). All point mutants of Par-3 and PTEN were prepared using the PCR-based method. Par-3 PDZ3-PTEN peptide fusion protein contained a thrombin cleavage site (LVPRGS) between the C terminus of PDZ3 and the PTEN peptide (DEDQSHQITKV).

Proteins were expressed in BL21 (DE3) *Escherichia coli* cells at either 37 or 16 °C. The His_6-tagged PDZ proteins were purified by Ni^{2+}-nitrilotriacetic acid-agarose (Qiagen) affinity chromatography followed by size exclusion chromatography. Uniformly isotope-labeled PDZ3 samples were prepared by growing bacteria in M9 minimal medium using $^{15}NH_4Cl$ as the sole nitrogen source or $^{15}NH_4Cl$ and $^{13}C_6$-glucose as the sole nitrogen and carbon sources, respectively. For *in vitro* GST pull-down-based assays, GST-PDZ3, GST-PTEN peptide, and their respective mutants were individually cloned into pGEX-4T-1 vector. The fusion proteins were purified by Glutathione-Sepharose-4B affinity chromatography (Amersham Biosciences). Myc9E10 monoclonal antibody was purchased from DSHB, anti-GFP antibody was from Invitrogen, and anti-PTEN polyclonal antibody and anti-rabbit horseradish peroxidase-conjugated secondary antibody were from Cell Signaling.

NMR Spectroscopy—The NMR samples were concentrated to ~0.1 mM (for titration experiments) or ~1 mM (for structural determinations) in 20 mM phosphate buffer, pH 6.0, 1 mM dithiothreitol, and 1 mM EDTA. NMR spectra were acquired at 30 °C on Varian Inova 500 or 750 MHz spectrometers, each equipped with a *z*-axis shielded triple resonance probehead. Sequential backbone and nonaromatic, nonexchangeable side chain resonance assignments of Par-3 PDZ3 alone and in complex with the PTEN peptide were achieved by standard heteronuclear correlation experiments, including HNCO, HNCACB, CBCA(CO)NH, and HCCH-TOCSY, using $^{15}N/^{13}C$-labeled samples, and confirmed by a three-dimensional ^{15}N-separated NOESY experiment using ^{15}N-labeled samples (32, 33). Except for the residues in the tag region, 100% backbone sequential resonance assignments were completed, and more than 98% nonaromatic side chain resonance assignments were obtained. The side chains of aromatics were further assigned by ^1H two-dimensional TOCSY and NOESY experiments using unlabeled samples in D_2O (34).

Structure Calculations—Approximate interproton distance restraints were derived from two-dimensional ^1H NOESY, three-dimensional ^{15}N-seperated NOESY, and three-dimensional ^{13}C-seperated NOESY spectra. NOE restraints were grouped into three distance ranges: 1.8–2.7 Å (1.8–2.9 Å for NOEs involving NH protons), 1.8–3.3 Å (1.8–3.5 Å for NOEs involving NH protons), and 1.8–5.0 Å, corresponding to strong, medium, and weak NOEs, respectively. Hydrogen bonding restraints were generated from the standard secondary structure of the protein based on the NOE patterns and backbone secondary chemical shifts. Backbone dihedral angle restraints (ϕ and ψ angles) were derived from the secondary structure of the protein and backbone chemical shift analysis program TALOS (35). Structures were calculated using the program CNS (36).

In Vitro Pull-down Assay—Aliquots of 50 μl of GST or GST-tagged proteins from 1 mg/ml stock solutions were first loaded to 20 μl of glutathione-Sepharose 4B slurry beads in an assay buffer containing 50 mM Tris-HCl, pH 7.5, 100 mM NaCl, and 1 mM dithiothreitol for 1 h at 4 °C. The GST fusion protein-loaded beads were washed twice with the assay buffer and then mixed with potential binding partners (purified recombinant proteins or HEK293T cell lysates overexpressed with GFP-tagged target proteins), and the mixtures were then incubated for 2 h at 4 °C. Beads were then washed three times each with 500 μl of the assay buffer. The proteins captured by the affinity beads were eluted by boiling, resolved by 15% SDS-PAGE, and detected either by Coomassie Blue staining or by immunoblotting with specific antibodies. In the pull-down assays, HEK293T cells transiently transfected with GFP-tagged proteins were lysed using radioimmune precipitation buffer (50 mM Tris-HCl, pH 7.4, 150 mM NaCl, 1% Nonidet P-40, 1 mM EDTA, 1 mM phenylmethylsulfonyl fluoride).

Fluorescence Polarization Assay—Fluorescence polarization assays were performed on a PerkinElmer Life Sciences LS-55 fluorimeter equipped with an automated polarizer at 20 °C. The PTEN synthetic peptide was labeled with fluorescein-5-isothiocyanate (Molecular Probes) at its N terminus. Fluorescence titration was performed by adding increasing amounts of Par-3 PDZ3 or its mutants to a constant amount of the fluorescein-5-isothiocyanate-PTEN peptide (~1 μM) in 50 mM HEPES buffer (pH 7.4) containing 100 mM NaCl, 1 mM EDTA, and 1 mM dithiothreitol. The dissociation constants (K_d) were obtained by fitting the titration curves with the classical one-site binding model using the software GraphPad. In this assay, $\Delta mP = mP - mP_0$, where mP is the measured polarization value of each titration point, and mP_0 is the polarization value of the free peptide.

RNA Interference and PTEN Knockdown—The sequences of the oligonucleotides used to knock down canine PTEN were designed using Dharmacon's online siDesign Center and inserted into pSUPER vector. Annealed double strand oligonucleotides were inserted into the BglII and HindIII cloning sites of the pSUPER vector. The two pairs of canine PTEN shRNA were designed as follows: sense primer for pSPTEN1, 5′-gatcc-ccCAGATAATGACAAGGAATA*TTCAAGAGA*TATTCCT-TGTCATTATCTGtttttggaaa-3′; antisense primer for pSPTEN1, 5′-agcttttccaaaaaCAGATAATGACAAGGAATA-*TCTCTTGAA*TATTCCTTGTCATTATCTGggg-3′; sense primer for pSPTEN2, 5′-gatccccAGTAAGGACCAGAGACA-AA*TTCAAGAGA*TTTGTCTCTTGGTCCTTACTtttttggaaa-3′; pSPTEN2 antisense primer, 5′-agcttttccaaaaaAGTAAGG-

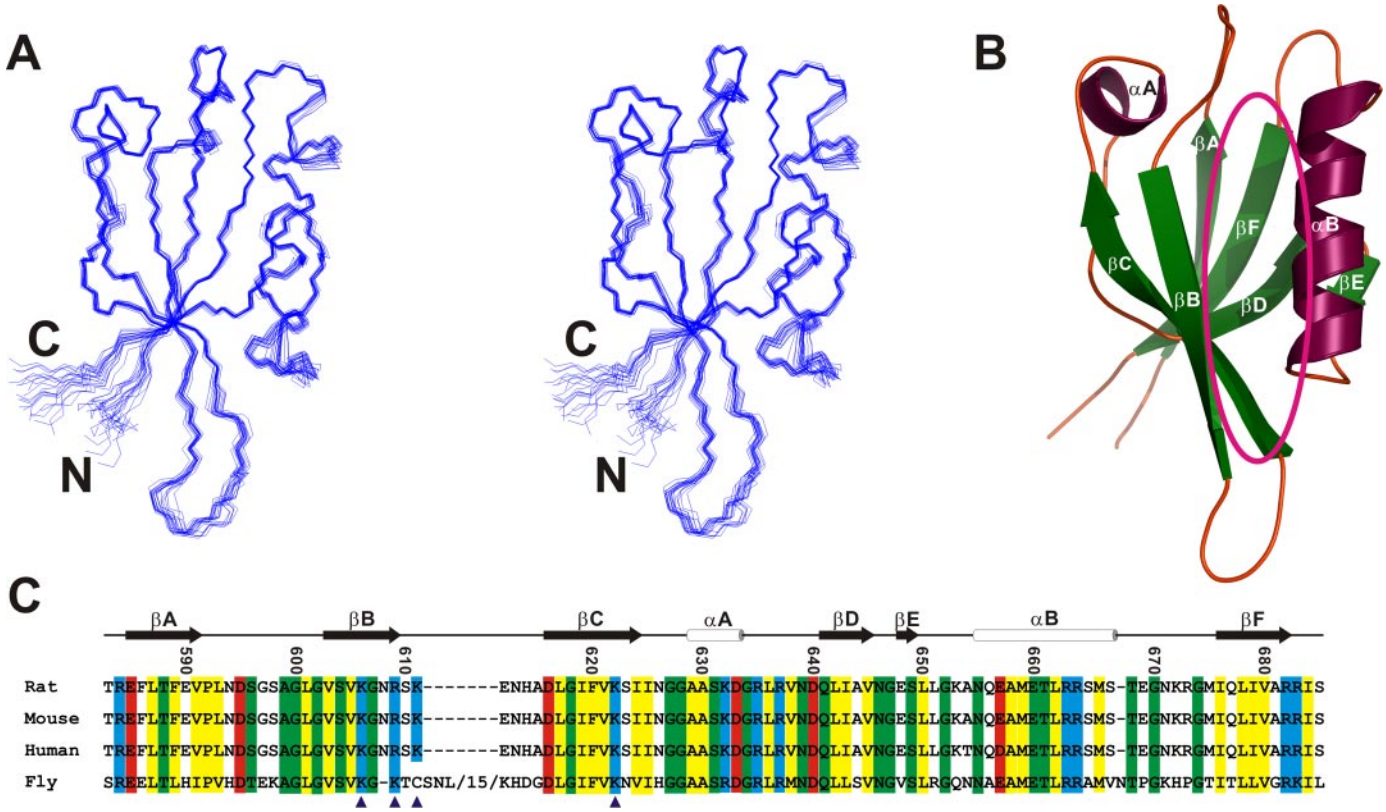

FIGURE 1. **Solution structure of Par-3 PDZ3.** *A*, stereoview showing the backbones of 20 superimposed NMR-derived structures of Par-3 PDZ3. *B*, *ribbon diagram* of a representative NMR structure of the Par-3 PDZ3. The secondary structure elements of PDZ3 are labeled according to the scheme used for the canonic PDZ domains. The potential peptide binding pocket is highlighted by a *magenta oval*. *C*, amino acid sequence alignment of the Par-3 PDZ3 from different species. The highly conserved hydrophobic, positively charged, and negatively charged residues are in *yellow*, *blue*, and *red*, respectively; other highly conserved residues are in *green*. The secondary structures of Par-3 PDZ3 and the residue number are marked at the *top* of the alignment. The positively charged residues responsible for the specific charge-charge interaction between PDZ3 and the PTEN peptide are highlighted by *blue triangles*. The protein structure figures were prepared using the programs MOLMOL (45), MOLSCRIPT (46), PyMOL (available on the World Wide Web), and GRASP (47).

ACCAGAGACAAA*TCTCTTGAA*TTTGTCTCTTGGTCC-TTACTggg-3′. Italic type indicates the 9-bp hairpin loop, and letters in lowercase represent the sequence designed for creating BglII and HindIII restriction digestion sites. Par-3-specific shRNA was designed as previously reported (25, 37). The empty pSUPER vector was used as a control for the PTEN knockdown. The following primary antibodies were used in the Western blot to assay the knockdown efficiency of PTEN: anti-PTEN polyclonal antibody (1:1000) (Cell Signaling), anti-occludin polyclonal antibody (1:1000) (Zymed Laboratories Inc.), and anti-β-tubulin monoclonal antibody (1:1000) (DSHB). Horseradish peroxidase-conjugated donkey anti-mouse (Jackson Laboratories) or donkey anti-rabbit secondary antibodies (Cell Signaling) were used at a concentration of 1:10000.

Cellular Localization and Stable Cell Line—The wild type Par-3 was cloned into the pEGFP-C2 vector, and the wild type PTEN was cloned into the pCMV-Myc vector. MDCK II cells were transiently co-transfected with 0.5 μg each of PTEN and Par-3 plasmids/well using the Lipofectamine™ *PLUS* kit (Invitrogen) and cultured for 48 h before fixation. HEK293T cells or MDCK II cells were cultured at 37 °C in minimal essential medium supplemented with 10% fetal bovine serum under a humidified atmosphere of 5% CO_2. MDCK cells stably expressing GFP-PLCδ PH were generated by selecting transfected cells with 500 μg/ml G418 as selection marker, and positive clones were maintained in normal cultural medium containing 250 μg/ml G418.

Calcium Switch Assay—Calcium switch experiments were performed as described previously (25). Briefly, pSPTEN1 was delivered using nucleotransfection kit (Amaxa) into cultured MDCK II cells with or without stably expressing GFP-PLCδ PH, along with the wild type PTEN or its mutants. After electroporation, ~7.5×10^5 MDCK II cells were seeded in a 24-well tissue culture plate with minimal essential medium containing 1.8 mM calcium (high calcium medium). After ~40 h of incubation, a confluent monolayer of MDCK cells was formed. Cells were washed twice with phosphate-buffered saline and incubated in minimal essential medium supplemented with 2% calf serum, which was dialyzed against 150 mM NaCl overnight (low calcium medium). After a 16-h incubation in low calcium medium, cells were switched back to HCM for the indicated time durations. To detect ZO-1, cells were washed then fixed in 4% paraformaldehyde for 15 min at room temperature and permeabilized with 0.2% Triton X-100 in phosphate-buffered saline. After washing with phosphate-buffered saline, cells were blocked with 10% normal donkey serum in phosphate-buffered saline for 1 h and incubated with anti-ZO-1 primary antibody and Red X-conjugated secondary antibody (anti-rabbit; Jackson Laboratory). The images were acquired and analyzed using a Nikon TE2000E inverted fluorescent microscope. Images were taken using a monochrome camera detection system, and composite *pseudocolors* are used in the merged figures for comparison.

TABLE 1

Structural statistics for the family of 20 structures of PDZ3 and PDZ-3 in complex with the PTEN peptide

None of the structures exhibits distance violations greater than 0.3 Å or dihedral angle violations greater than 4°.

Parameters	Values	
	PDZ3	PDZ3-PTEN peptide
Distance restraints		
Intraresidue ($i - j = 0$)	831	888
Sequential ($\|i - j\| = 1$)	562	578
Medium range ($2 < \|i - j\| < 4$)	368	366
Long range($\|i - j\| > 5$)	771	877
Hydrogen bonds	78	94
Total	2,610	2,803
Dihedral angle restraints		
Φ	50	55
Ψ	51	55
Total	101	110
Mean root mean square deviations from the experimental restraints		
Distance (Å)	0.014 ± 0.001	0.013 ± 0.000
Dihedral angle (degrees)	0.197 ± 0.036	0.324 ± 0.034
Mean root mean square deviations from idealized covalent geometry		
Bond (Å)	0.002 ± 0.000	0.002 ± 0.000
Angle (degrees)	0.336 ± 0.007	0.370 ± 0.004
Improper (degrees)	0.227 ± 0.011	0.249 ± 0.010
Mean energies (kcal mol^{-1})[a]		
E_{NOE}	25.13 ± 2.50	24.83 ± 1.49
E_{cdih}	0.25 ± 0.09	0.71 ± 0.15
$E_{L\text{-}J}$	−202.74 ± 7.81	−284.19 ± 10.75
Ramachandran plot[b] **(residues 582–685 in PDZ3; 393–403 in PTEN)**		
Percentage of residues in most favorable regions	72.2	72.2
Percentage of residues in additional allowed regions	21.9	24.7
Percentage of residues in generously allowed regions	5.1	2.7
Atomic root mean square differences (Å); full molecule (residues 585–682 in PDZ3; 393–395 and 400–403 in PTEN)		
Backbone heavy atoms (N, C$^{\alpha}$, and C′)	0.36	0.36
Heavy atoms	0.85	0.72

[a] The final values of the square well NOE and dihedral angle potentials were calculated with force constants of 50 kcal mol^{-1} Å^{-1} and 200 kcal mol^{-1} rad^{-1}.
[b] The program PROCHECK (48) was used to assess the overall quality of the structures.

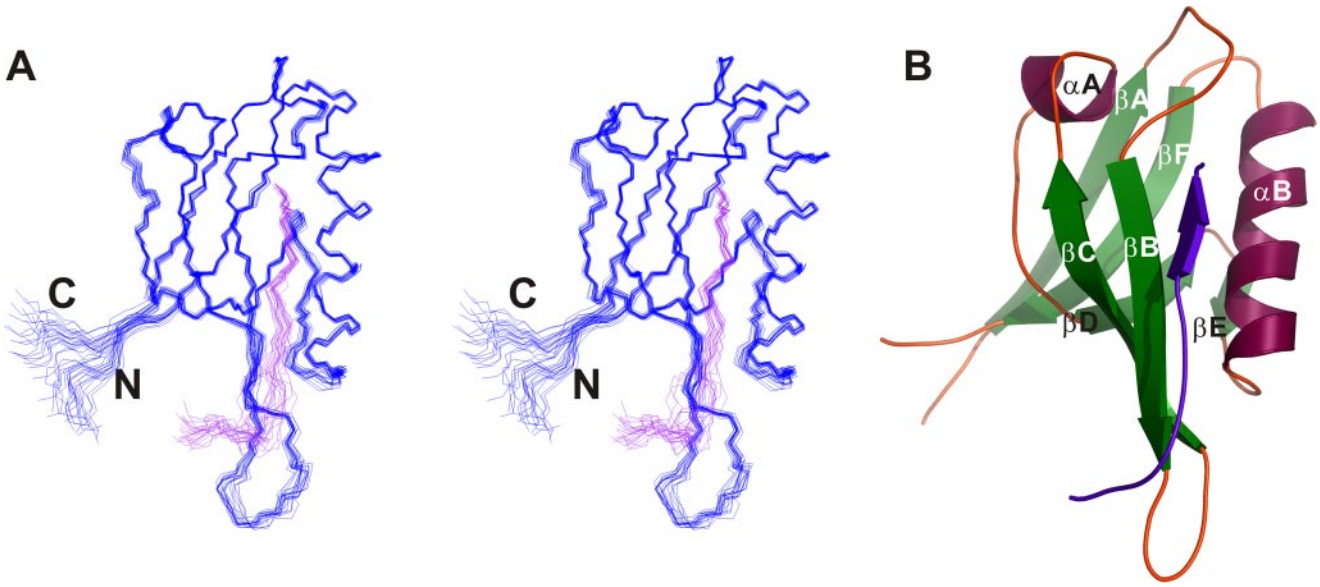

FIGURE 2. **Structure of Par-3 PDZ3 in complex with the PTEN peptide.** *A*, stereoview of the backbones of 20 superimposed NMR-derived structures of Par-3 PDZ3 in complex with the PTEN peptide. The PTEN peptide is shown in *purple*. *B*, *ribbon diagram* of a representative NMR structure of the Par-3 PDZ3-PTEN peptide complex. The PTEN peptide is *colored* as in *A*.

RESULTS AND DISCUSSION

Overall Structure of Par-3 PDZ3—As the first step in elucidating the molecular basis of the Par-3/PTEN interaction, we determined the solution structure of the ligand-free form of Par-3 PDZ3 using NMR spectroscopy. Except for a few residues in the two termini, the overall structure of Par-3 PDZ3 is well defined (Fig. 1*A* and Table 1). Par-3 PDZ3 adopts the canonical PDZ domain fold composed of six β-strands and two α-helices, of which the six β-strands form a partially open barrel with each of the open ends capped with an α-helix (Fig. 1*B*). Uniquely, the αB helix of Par-3 PDZ3 is one turn longer than the corresponding helix in the canonical PDZ domains (Fig. 1*B*). Parallel to the

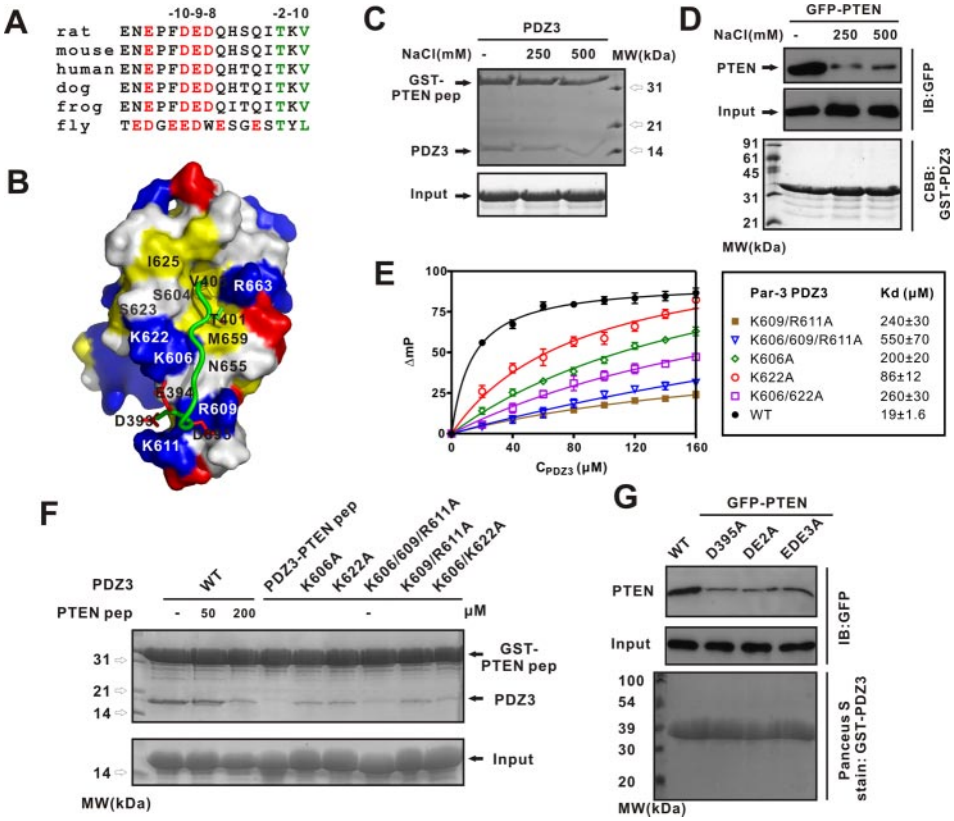

FIGURE 3. **Charge-charge interaction plays critical roles in the formation of the PDZ3-PTEN complex.** *A*, amino acid sequence alignment of the PTEN C-terminal tail across different species. The conserved PDZ domain-binding motif residues are *colored* in *green*; the conserved negative charge clustered residues are *colored* in *red*. *B*, the interface between the PTEN peptide and Par-3 PDZ3. Par-3 PDZ3 is shown using surface representation. The hydrophobic residues are drawn in *yellow*, positively charged residues in *blue*, negatively charged residues in *red*, and others in *gray*. The PTEN peptide is shown with the worm model. The side chains of the residues in PDZ-binding motif and three negatively charged residues ($^{-10}$DED^{-8}) of the peptide are shown in a *stick representation*. *C* and *D*, salt concentration-dependent interaction between Par-3 PDZ3 and PTEN. *C*, GST-fused PTEN peptide (DEDQHSQITKV) was used to pull down purified Par-3 PDZ3 dissolved in assay buffer containing 0, 250, and 500 mM NaCl, respectively. *Input*, represents 10% total PDZ3 used in the assay. Proteins in this assay were visualized with Coomassie Blue staining. *D*, purified GST-PDZ3 was used to pull down GFP-tagged full-length PTEN expressed in HEK293T cells in the presence of increasing concentrations of NaCl in the assay buffer. PTEN bound to Par-3 PDZ3 was visualized by immunodetection using anti-GFP antibody (immunoblot; *IB*). The amount of GST-PDZ3 in this assay is indicated with Coomassie Blue (*CBB*) staining of the protein. The input of GFP-PTEN represents 10% of the total GFP-PTEN used in the assay. *E*, measurements of the binding affinities between the PTEN peptide and various forms of Par-3 PDZ3 using fluorescence polarization assay. Neutralization of the positively charged residues on PDZ3 (Lys^{606}, Lys^{609}, Arg^{611}, and Lys^{622}) significantly reduced the binding of the domain to the PTEN peptide. *F*, mutational analysis of the roles of the positively charged residues in Par-3 PDZ3 in binding to PTEN. Synthetic PTEN peptide competes with the GST-fused PTEN peptide in binding to Par-3 PDZ3 in a dose-dependent manner. The *panel* also shows that mutation of the positively charged residues in Par-3 PDZ3 greatly reduced its binding to the PTEN peptide. The PDZ3-PTEN peptide fusion protein was included as the negative control of the assay, since the ligand binding pocket of Par-3 PDZ3 is completely blocked by the fused PTEN peptide. *G*, the $^{-10}$DED^{-8} motif of PTEN is critical for Par-3 binding. Mutations of the $^{-10}$DED^{-8} motif in the full-length PTEN also reduced its binding to GST-PDZ3. The amount of GST-PDZ3 used in the assay (*Input*) was shown by Ponceau-S staining. *Input* in *F* and *G* represents 25% of the proteins used in the assays. *WT*, wild type.

elongation of the αB helix, both βB and βC of Par-3 PDZ3 are longer than the corresponding β-strands in most PDZ domains. Therefore, the peptide ligand-binding channel of Par-3 PDZ3 is significantly elongated (Fig. 1*B*). Additionally, both the βA/βB-loop and the βB/βC-loop of the ligand-free Par-3 PDZ3 are well structured (Fig. 1*A*), indicating that the ligand binding groove of the domain is preformed and relatively rigid. Analysis of the molecular surface property of Par-3 PDZ3 revealed that the domain contains a prominent positively charged surface formed by four conserved residues (Lys^{606}, Arg^{609}, Lys^{611}, and Lys^{622}) at the distal end (with respect to the characteristic carboxyl-binding GLGF motif) of the peptide ligand-binding channel (supplemental Fig. 1). These distinct structural features of Par-3 PDZ3 are important for its target recognition specificity (see below for details).

Structure of Par-3 PDZ3 in Complex with the PTEN C-terminal Tail Peptide—Our earlier biochemical studies demonstrated that the carboxyl tail of PTEN is directly involved in binding to Par-3 PDZ3 (25). To characterize the interaction between Par-3 PDZ3 and PTEN C-terminal tail in further detail, we titrated the ^{15}N-labeled Par-3 PDZ3 with a synthetic peptide composed of the last 10 amino acids of PTEN (referred to hereafter as the PTEN peptide). The addition of the PTEN peptide induced large chemical shift changes to a subset of peaks of PDZ3, indicating that the PTEN peptide binds specifically to the PDZ domain. We then mapped the PTEN peptide binding-induced chemical shift changes of the Par-3 PDZ domain onto its three-dimensional structure (supplemental Fig. 2). As expected, residues in the predicted peptide ligand binding αB/βB-groove underwent prominent PTEN peptide binding-induced chemical shift changes, indicating that the PDZ domain binding motif at the extreme carboxyl end of the PTEN peptide (*i.e.* TKV) is directly involved in binding to the PDZ domain via the classical PDZ-peptide interaction mode (38). Interestingly, the PTEN peptide binding-induced chemical shift changes of Par-3 PDZ3 extend beyond the residues in the αB/βB-groove. Specifically, Lys^{606}, Arg^{609}, Lys^{611}, and Lys^{622}, which form the positively charged surface cluster, also showed significant chemical shift changes (supplemental Fig. 2). Amino acid sequence alignment analysis of PTEN from various species revealed that the three residues preceding the extreme carboxyl terminus are highly conserved acidic amino acids (see Fig. 3*A*), suggesting that these negatively charged residues might be interacting with the residues in the positively charged surface cluster of Par-3 PDZ3.

To elucidate the detailed interaction mechanism between Par-3 PDZ3 and PTEN, we decided to determine the structure of Par-3 PDZ3 in complex with the PTEN peptide. First, we

validated that the last 10 residues of PTEN are sufficient for binding to Par-3 PDZ3, since further extension of the peptide toward the N terminus did not enhance the binding affinity between Par-3 PDZ3 and PTEN (data not shown). To facilitate the NMR-based structural determination of the Par-3 PDZ3-PTEN peptide complex, we fused the PTEN peptide to the C terminus of Par-3 PDZ3 to generate a single chain fusion protein. This strategy greatly simplified the complex structure determination. The same strategy has been successfully used in determining the structures of a number of other PDZ domains in complex with their respective target peptides (39, 40). Additionally, the NMR spectrum of Par-3 PDZ3 in complex with the synthetic PTEN peptide and that of the PDZ3-PTEN peptide fusion protein are essentially identical, indicating that the covalent linking of the PTEN peptide to the PDZ domain has minimal perturbation to the structure of the Par-3 PDZ3-PTEN peptide complex (supplemental Fig. 3).

The structure of the Par-3 PDZ3-PTEN peptide complex was determined to a high resolution (Fig. 2*A* and Table 1). The structure of PDZ3 in the complex is highly similar to the structure of the ligand free Par-3 PDZ3 (root mean square deviation of 0.9 comparing the backbones of the two structures). The only notable peptide binding-induced conformational change of Par-3 PDZ3 is the rotation of αB, since this rotation is necessary to widen the αB/βB-groove in order to accommodate the PTEN peptide (supplemental Fig. 4). Consistent with our earlier prediction, the three residues at the extreme C terminus of the PTEN peptide form a β-strand that pairs in an antiparallel manner with the βB of PDZ3. The side chain of the residue at the 0-position of the PTEN peptide (Val^{403}) packs tightly into the pocket formed by Leu^{601}, Val^{603}, Leu^{662}, and Met^{666}. Due to the elongated αB-helix of Par-3 PDZ3, the residue at the −2-position (Thr^{401}) of the PTEN peptide interacts, albeit weakly, with the side chain of Met^{659} (the fifth residue in the αB) instead of Asn^{655} at the αB1 position of Par-3 PDZ3 (Fig. 3*B*) (38). No specific hydrogen bonding between the side chain of Thr^{403} from the PTEN peptide and the residues from the αB-helix of Par-3 PDZ3 could be observed. The side chain of Lys^{402} (the so-called −1 residue) from the PTEN peptide also lacks direct contact with Par-3 PDZ3. As a distinct property of the Par-3 PDZ3-PTEN peptide complex, the three negatively charged residues at the N-terminal end of the PTEN peptide ($^{-10}$DED^{-8}) directly interact with a cluster of positively charged residues (Lys^{606}, Arg^{609}, Lys^{611}, and Lys^{622}) from the βB, βC, and βB/βC loop of Par-3 PDZ3 (Figs. 1*C* and 3*B*). This unique charge-charge interaction is predicted to enhance the binding affinity and, perhaps more importantly, to provide the binding specificity between Par-3 PDZ3 and PTEN (*i.e.* the interaction between Par-3 PDZ3 and PTEN requires the presence of both the classical PDZ-binding motif at the extreme tail and the upstream $^{-10}$DED^{-8} motif of PTEN).

The Charge-Charge Interaction in the Formation of the PDZ3-PTEN Complex—We next tested the role of the charge-charge interaction, shown in Fig. 3*B*, in the formation of the Par-3 PDZ3-PTEN complex. In a pull-down assay, the binding of GST-fused PTEN peptide to Par-3 PDZ3 weakened when the salt concentration in the assay buffer was increased (Fig. 3*C*). Similarly, the interaction between GST-fused Par-3 PDZ3 and the full-length PTEN expressed in HEK293T cells was also salt concentration-dependent (Fig. 3*D*). To test that the positively charged residues in the βB-, βC-, and βB/βC-loop of Par-3 PDZ3 shown in Fig. 3*B* are required for binding to PTEN, we substituted individual or multiple positively charged residues with neutral Ala and measured the binding of each mutant to the PTEN peptide using fluorescence spectroscopy and affinity pull-down assays (Fig. 3, *E* and *F*). The data clearly demonstrated that these positively charged residues play important roles in promoting the formation of the Par-3 PDZ3-PTEN peptide complex, since substitution of single or multiple positively charged residues significantly decreased the binding of

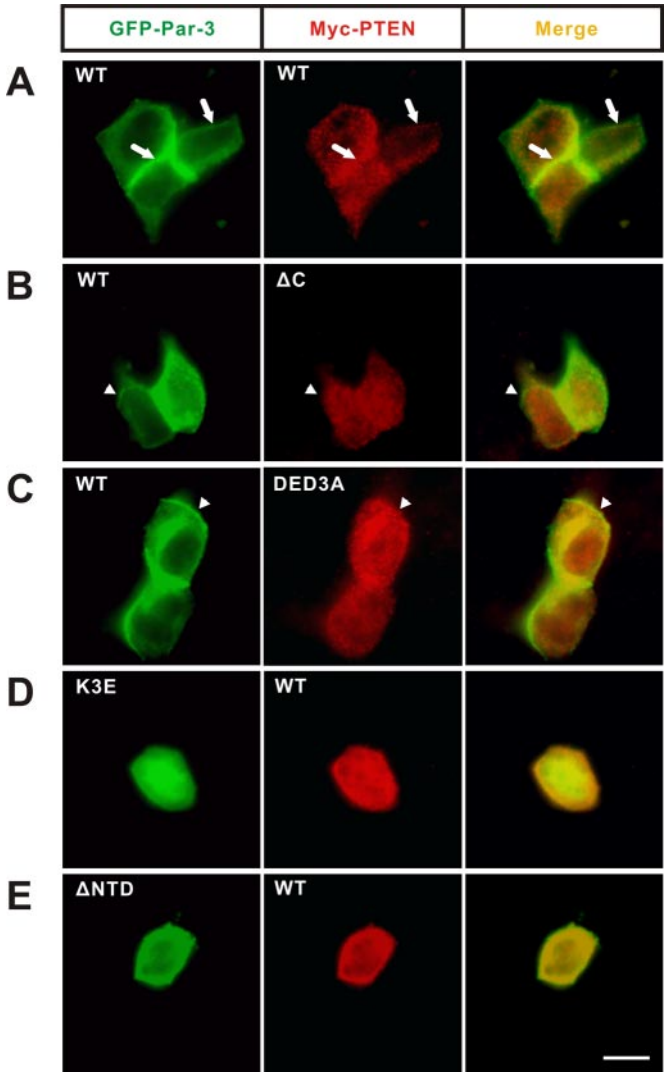

FIGURE 4. **Par-3 enriches PTEN at the junctional membranes via its PDZ3 domain.** *A*, overexpressed Par-3 was specifically enriched at the junctional membrane in polarized epithelial cells, and PTEN was partially colocalized with Par-3 (*white arrows*). In this experiment, MDCK II cells were transiently co-transfected with GFP-Par-3 and Myc-PTEN. *B*, C-terminal tail deletion mutant of PTEN failed to colocalize with Par-3 at the junctional membrane regions (*arrowhead*). *C*, the DED3A mutant of PTEN also failed to colocalize with Par-3 at the membrane junctions (*arrowhead*). Instead, the PTEN mutant is diffused in the cytoplasm. *D*, PDZ2 lipid binding-deficient mutant of Par-3 (K3E) is diffused in cytoplasm (25). Co-expressed PTEN is also absent at the junctional membranes. *E*, the oligomerization-deficient mutant of Par-3 (ΔNTD) (21) is diffused in MDCK cells. Co-expressed PTEN is also missing from the junctional membranes. Note that the Par-3 mutants in *D* and *E* retain the PTEN binding capacities. *Scale bar*, 10 μm. *WT*, wild type.

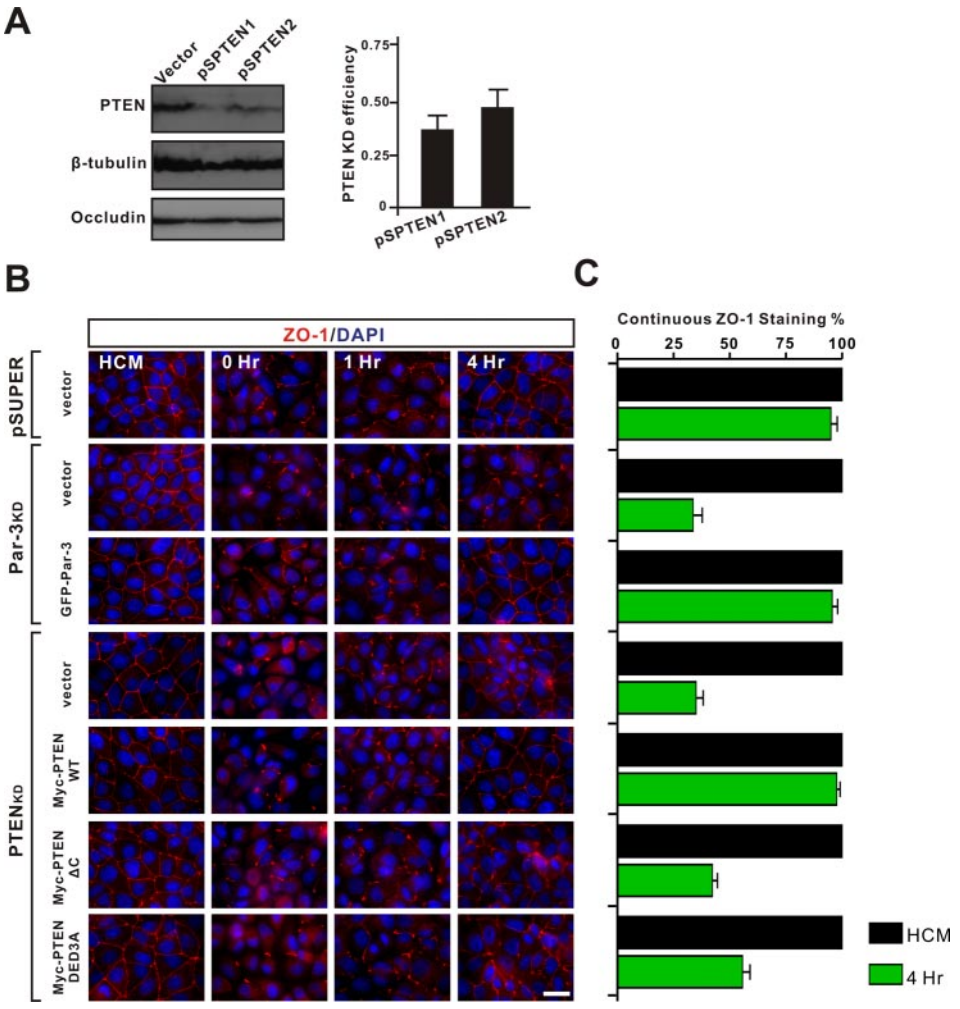

FIGURE 5. **Junctional membrane-localized PTEN is required for epithelial cell polarization.** *A*, knockdown of endogenous canine PTEN with pSUPER-based shRNA. MDCK II cells were transiently transfected with the empty pSUPER vector (control), pSPTEN1, and pSPTEN2, respectively. pSPTEN1 knocked down ~65% of the PTEN expression, and pSPTEN2 reduced ~50% of the PTEN expression. The figure also shows that PTEN knockdown did not alter the expression level of the tight junction protein occludin. β-Tubulin was used as the loading controls. *Error bars*, S.D. of three different experiments. *B*, rescue of the polarization defects of MDCK cells induced by PTEN knockdown with various RNA interference-resistant rat PTEN constructs. MDCK cells were transfected with pSUPER vector, pSPar-3, and pSPTEN1 together with various rescue constructs as indicated. Cells were subjected to the "calcium switch" assay and fixed at the indicated time points after the calcium switch (0, 1, and 4 h). 4′,6-diamidino-2-phenylindole (*blue*) was used to stain nuclei and served for counting the cell numbers in each assay, and ZO-1 (*red*) was used to monitor the tight junction formation. *Scale bar*, 20 μm. *C*, quantification of cells in the rescue experiments with continuous ZO-1 staining. *Black bars*, continuous ZO-1 staining in fully polarized MDCK cells cultured in HCM. *Green bars*, percentage of the cells with continuous ZO-1 staining 4 h after cells were switched back to the normal calcium medium. Data were derived from counting of 100 cells in three randomly selected fields under a microscope. *Error bar*, S.D. from three different experiments.

Par-3 PDZ3 to PTEN. The CD spectra of all these charge neutralization mutants are essentially the same as that of the wild type protein, indicating that the weakened PTEN bindings of the mutants were not the artifact of mutation-induced conformation alterations (supplemental Fig. 5). Reciprocally, we made point mutations on the PTEN by converting one or multiple negatively charged residues in the $^{-10}$DED^{-8} motif to Ala and subsequently assayed the binding of the PTEN mutants to GST-PDZ3 using pull-down experiments. Consistent with our structural analysis, the point mutations of PTEN also showed significantly weakened binding to Par-3 PDZ3 (Fig. 3*G*). Taken together, the data shown in Fig. 3 demonstrate that the charge-charge interaction between the positively charged surface cluster of Par-3 PDZ3 and the $^{-10}$DED^{-8} motif of PTEN plays an instructive role for the complex formation. The presence of two discrete binding sites (the canonical PDZ-binding site and the distal charge-charge interaction site) seen in the Par-3 PDZ3-PTEN peptide complex is unique when compared with all currently known PDZ-ligand complexes. The formation of the Par-3·PTEN complex is thus likely to be specific when compared with other potential PTEN-binding PDZ domain proteins, including MAGI-2, MAGI-3 (41, 42), and NHERF (43). Amino acid sequence analysis of the PDZ domains of MAGI-2, MAGI-3, and NHERF indicated that these PDZ domains do not contain the second charge-charge interaction site seen in the Par-3 PDZ3-PTEN complex (results not shown).

Par-3 Enriches PTEN at Junctional Membranes via Its PDZ3 Domain—We next studied the role of the Par-3/PTEN interaction in the regulation of cell polarity. We first compared the cellular localizations of the wild type PTEN with those of Par-3 PDZ3 binding-deficient PTEN in MDCK cells. Consistent with earlier reports (21, 25, 37), overexpressed GFP-tagged wild type Par-3 is mainly localized at the membrane junctions of MDCK cells (Fig. 4*A*). Myc-tagged PTEN, on the other hand, is mainly diffused, with partial enrichment at the membrane junctions (Fig. 4*A*). This observation is consistent with the data reported earlier (31, 44), and is in line with the modest binding affinity observed between Par-3 PDZ3 and PTEN (Fig. 2) and ubiquitous cellular functions of PTEN. The removal of the last 10 residues of PTEN (PTENΔC) led to the complete diffusion of PTEN in MDCK cells, presumably due to the disruption of Par-3 PDZ3-mediated PTEN binding (Fig. 4*B*). The truncation of the C-terminal 10 residues of PTEN could have a potential caveat, since the truncation may also disrupt PTEN binding to other potential membrane-associated PDZ domain proteins. Since the charge-charge interaction between the $^{-10}$DED^{-8} motif of PTEN and the positively charged surface cluster outside the canonical ligand binding groove of Par-3 PDZ3 is unique to the Par-3·PTEN complex, mutation of the negatively charged $^{-10}$DED^{-8} in PTEN to AAA (DED3A) can be expected to disrupt Par-3/PTEN interaction

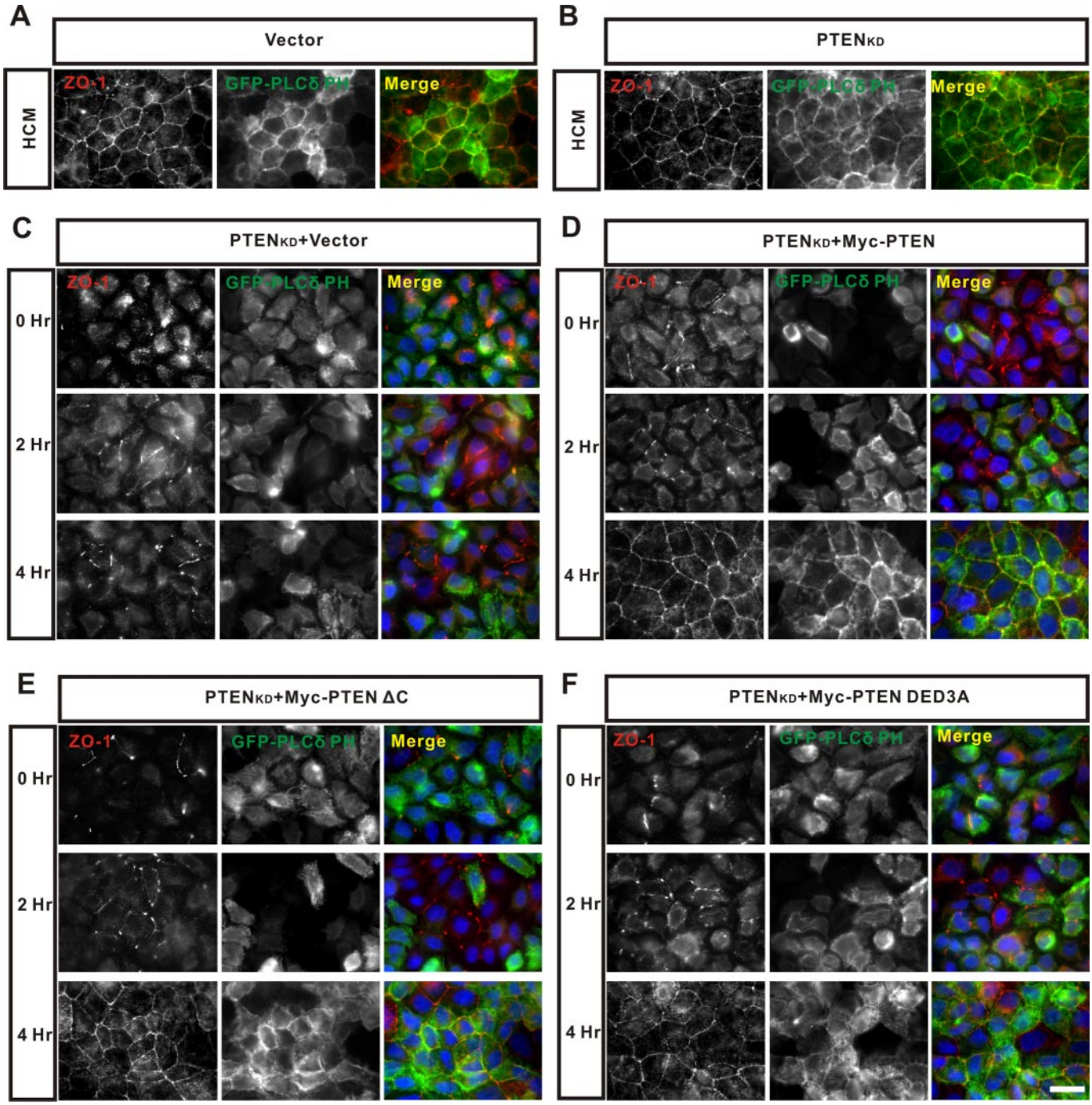

FIGURE 6. **Junctional membrane enrichment of PTEN via Par-3 is critical for PI(4,5)P2 distribution in polarizing epithelial cells.** *A* and *B*, MDCK cells stably expressing GFP-PLCδ PH domain were transfected with pSUPER (*A*, vector) and pSPTEN1 (*B*, $PTEN_{KD}$). When transfected cells were cultured in HCM for a sufficiently long time (*e.g.* 48 h), knockdown of PTEN by pSPTEN1 had no obvious defect in cell polarity. The data also showed that PI(4,5)P2 is highly enriched and co-localized with ZO-1 in the junctional membranes in the polarized cells. *C*, knockdown of endogenous PTEN severely delayed repolarization of MDCK cells. After switching the cells from the low calcium medium to normal calcium medium, repolarization of MDCK cells was assayed by staining the tight junction marker ZO-1 at the indicated time points. The $PTEN_{KD}$ MDCK cells failed to repolarize even 4 h after calcium switch. In these cells, PI(4,5)P2 is abnormally segregated, as indicated by the GFP-PLCδ PH biosensor. *D*, co-transfection of the Myc-tagged wild type rat PTEN fully rescued the polarization defects induced by the knockdown of endogenous PTEN. In the rescued cells, PI(4,5)P2 is concentrated in the junctional membranes together with ZO-1. *E* and *F*, the Par-3 binding-deficient mutants of PTEN (ΔC and DED3A) were not able to rescue the repolarization defect of the MDCK cells caused by the knock-down of the endogenous PTEN. In parallel, PI(4,5)P2 was also mislocalized from the junctional membrane regions in PTEN(ΔC)- and PTEN(DED3A)-transfected cells. *Scale bar*, 20 μm.

specifically while leaving other potential PTEN/PDZ interaction intact. In MDCK cells, the DED3A mutant of PTEN is also largely diffused (Fig. 4*C*), indicating that the specific Par-3 PDZ3-PTEN interaction is responsible for the enrichment of PTEN in membrane junctions. Based on the above data, one can predict that the disruption of Par-3 junctional membrane localization should also disrupt the membrane enrichment of PTEN. We earlier reported that the disruption of either PDZ2-mediated lipid membrane interaction or NTD-mediated oligomerization of Par-3 led to the complete diffusion of the protein in

MDCK cells (21, 25). When co-expressed with either of these two Par-3 mutants, PTEN is completely diffused in the cytosol (Fig. 4, *D* and *E*). In summary, the above data demonstrate that the partial membrane localization of PTEN requires the Par-3 PDZ3-PTEN interaction.

Par-3 PDZ3-PTEN Interaction Is Required for Epithelial Cell Polarity—We next tested the role of the Par-3 PDZ3-mediated junctional membrane localization of PTEN in the polarization of MDCK cells. The disruption of Par-3 PDZ3-PTEN interaction was predicted to interfere with the polarization of MDCK cells if the junctional population of PTEN is functionally important. To test this hypothesis, we first knocked down the endogenous PTEN using the RNA interference approach and then compared the capacities of various PTEN mutants in rescuing the function of the wild type PTEN using a "calcium switch"-based MDCK cell repolarization assay. The two shRNAs against PTEN, pSPTEN1, and pSPTEN2 showed specific knockdown of endogenous canine PTEN (Fig. 5*A*). Since the pSPTEN1 was somewhat more effective in knocking down the wild type PTEN, this shRNA was used for the subsequent MDCK repolarization assay. In normal calcium-containing medium, MDCK cells transfected with shRNA specific to PTEN ($PTEN_{KD}$) will eventually fully polarize (*e.g.* 48 h after transfection) as indicated by ZO-1 staining (Fig. 5*B*, *HCM*). However, knockdown of PTEN significantly delayed repolarization of MDCK cells after the "calcium switch." This repolarization defect caused by the reduced expression of PTEN was phenotypically copied by knockdown of Par-3, consistent with our biochemical data showing that Par-3 is responsible for bringing PTEN to the junctional membranes (Fig. 5*B*). As expected, the expression of small interfering RNA-resistant human PTEN fully rescued the repolarization defect of MDCK induced by the RNA interference knockdown of endogenous PTEN (Fig. 5, *B* and *C*). In contrast, neither PTEN(ΔC) nor PTEN("DED3A") could rescue the repolarization defect of MDCK cells (Fig. 5, *B* and *C*).

We next used the PH domain from PLCδ as a PI(4,5)P2 biosensor to monitor the junctional membrane PI(4,5)P2. In MDCK cells stably expressing GFP-PLCδ PH, the colocalization of PLCδ PH with tight junction marker protein ZO-1 suggested that PI(4,5)P2 is highly enriched at the junctional membrane region in polarized MDCK cells (Fig. 6*A*, *HCM*). Reduced expression of endogenous PTEN by shRNA had a limited effect on both tight junction formation and PI(4,5)P2 junctional membrane enrichment in normal medium (Fig. 6*B*), presumably due to the limited knockdown of the phosphatase activity. In the "calcium switch" assay, depletion of Ca^{2+} not only caused the dissolution of ZO-1 but also disrupted the defined PI(4,5)P2 junctional localization (Fig. 6, *C–F*). Expression of the shRNA-resistant wild type PTEN fully rescued the junctional enrichment defects of PI(4,5)P2 and the delayed repolarization of MDCK cells induced by the knockdown of the endogenous PTEN (Fig. 6*D*). In contrast, PTEN(ΔC) and PTEN(DED3A) failed to restore the junctional localization of PI(4,5)P2 (Fig. 6, *E* and *F*).

Taken together, the above data strongly support our conclusion that the Par-3 PDZ3-mediated PTEN junctional membrane localization is important in the regulation of epithelial cell polarization. Our study also supports our earlier model that the PDZ3-mediated PTEN membrane localization plays important roles in metabolism as well as asymmetric distributions of PI(4,5)P2 and phosphatidylinositol 3,4,5-trisphosphate in polarized cell membranes (25).

In summary, we have elucidated the molecular basis of Par-3/PTEN interaction by the determination of the solution structures of Par-3 PDZ3 alone and in complex with the PTEN peptide. We demonstrated that the Par-3 PDZ3-mediated junctional membrane enrichment of PTEN is critical for epithelial cell polarization and for the enrichment of PI(4,5)P2 in junctional membranes. The data presented in this study provide a mechanistic connection between phosphoinositide signaling and the Par-3·Par-6·aPKC complex in the context of cell polarity regulation.

Acknowledgment—We thank Mr. Anthony Zhang for careful reading of the manuscript.

REFERENCES

1. Drubin, D. G., and Nelson, W. J. (1996) *Cell* **84,** 335–344
2. Knoblich, J. A. (2001) *Nat. Rev. Mol. Cell. Biol.* **2,** 11–20
3. Wodarz, A. (2002) *Nat. Cell Biol.* **4,** E39–E44
4. Nelson, W. J. (2003) *Nature* **422,** 766–774
5. Macara, I. G. (2004) *Nat. Rev. Mol. Cell. Biol.* **5,** 220–231
6. Jan, Y. N., and Jan, L. Y. (2000) *Cell* **100,** 599–602
7. Kemphues, K. (2000) *Cell* **101,** 345–348
8. Ohno, S. (2001) *Curr. Opin. Cell Biol.* **13,** 641–648
9. Pellettieri, J., and Seydoux, G. (2002) *Science* **298,** 1946–1950
10. Shin, K., Fogg, V. C., and Margolis, B. (2006) *Annu. Rev. Cell Dev. Biol.* **22,** 207–235
11. Arimura, N., and Kaibuchi, K. (2007) *Nat. Rev. Neurosci.* **8,** 194–205
12. Macara, I. G. (2004) *Curr. Biol.* **14,** R160–R162
13. Margolis, B., and Borg, J. P. (2005) *J. Cell Sci.* **118,** 5157–5159
14. Suzuki, A., and Ohno, S. (2006) *J. Cell Sci.* **119,** 979–987
15. Goldstein, B., and Macara, I. G. (2007) *Dev. Cell* **13,** 609–622
16. Etemad-Moghadam, B., Guo, S., and Kemphues, K. J. (1995) *Cell* **83,** 743–752
17. Hung, T. J., and Kemphues, K. J. (1999) *Development* **126,** 127–135
18. Joberty, G., Petersen, C., Gao, L., and Macara, I. G. (2000) *Nat. Cell Biol.* **2,** 531–539
19. Lin, D., Edwards, A. S., Fawcett, J. P., Mbamalu, G., Scott, J. D., and Pawson, T. (2000) *Nat. Cell Biol.* **2,** 540–547
20. Qiu, R. G., Abo, A., and Steven Martin, G. (2000) *Curr. Biol.* **10,** 697–707
21. Feng, W., Wu, H., Chan, L. N., and Zhang, M. (2007) *EMBO J.* **26,** 2786–2796
22. Chan, J. R., Jolicoeur, C., Yamauchi, J., Elliott, J., Fawcett, J. P., Ng, B. K., and Cayouette, M. (2006) *Science* **314,** 832–836
23. Itoh, M., Sasaki, H., Furuse, M., Ozaki, H., Kita, T., and Tsukita, S. (2001) *J. Cell Biol.* **154,** 491–497
24. Takekuni, K., Ikeda, W., Fujito, T., Morimoto, K., Takeuchi, M., Monden, M., and Takai, Y. (2003) *J. Biol. Chem.* **278,** 5497–5500
25. Wu, H., Feng, W., Chen, J., Chan, L. N., Huang, S., and Zhang, M. (2007) *Mol. Cell* **28,** 886–898
26. Pinal, N., Goberdhan, D. C., Collinson, L., Fujita, Y., Cox, I. M., Wilson, C., and Pichaud, F. (2006) *Curr. Biol.* **16,** 140–149
27. von Stein, W., Ramrath, A., Grimm, A., Muller-Borg, M., and Wodarz, A. (2005) *Development* **132,** 1675–1686
28. Toyoshima, F., Matsumura, S., Morimoto, H., Mitsushima, M., and Nishida, E. (2007) *Dev. Cell* **13,** 796–811
29. Leslie, N. R., Yang, X., Downes, C. P., and Weijer, C. J. (2007) *Curr. Biol.* **17,** 115–125
30. Comer, F. I., and Parent, C. A. (2007) *Cell* **128,** 239–240

31. Martin-Belmonte, F., Gassama, A., Datta, A., Yu, W., Rescher, U., Gerke, V., and Mostov, K. (2007) *Cell* **128,** 383–397
32. Bax, A., and Grzesiek, S. (1993) *Acc. Chem. Res.* **26,** 131–138
33. Kay, L. E., and Gardner, K. H. (1997) *Curr. Opin. Struct. Biol.* **7,** 722–731
34. Wuthrich, K. (1986) *NMR of Proteins and Nucleic Acids*, John Wiley & Sons, Inc., New York
35. Cornilescu, G., Delaglio, F., and Bax, A. (1999) *J. Biomol. NMR* **13,** 289–302
36. Brunger, A. T., Adams, P. D., Clore, G. M., DeLano, W. L., Gros, P., Grosse-Kunstleve, R. W., Jiang, J. S., Kuszewski, J., Nilges, M., Pannu, N. S., Read, R. J., Rice, L. M., Simonson, T., and Warren, G. L. (1998) *Acta Crystallogr. D Biol. Crystallogr.* **54**, 905–921
37. Chen, X., and Macara, I. G. (2005) *Nat. Cell Biol.* **7,** 262–269
38. Zhang, M., and Wang, W. (2003) *Acc. Chem. Res.* **36,** 530–538
39. Elkins, J. M., Papagrigoriou, E., Berridge, G., Yang, X., Phillips, C., Gileadi, C., Savitsky, P., and Doyle, D. A. (2007) *Protein Sci.* **16,** 683–694
40. Pan, L., Wu, H., Shen, C., Shi, Y., Jin, W., Xia, J., and Zhang, M. (2007) *EMBO J.* **26,** 4576–4587
41. Wu, Y., Dowbenko, D., Spencer, S., Laura, R., Lee, J., Gu, Q., and Lasky, L. A. (2000) *J. Biol. Chem.* **275,** 21477–21485
42. Wu, X., Hepner, K., Castelino-Prabhu, S., Do, D., Kaye, M. B., Yuan, X. J., Wood, J., Ross, C., Sawyers, C. L., and Whang, Y. E. (2000) *Proc. Natl. Acad. Sci. U. S. A.* **97,** 4233–4238
43. Takahashi, Y., Morales, F. C., Kreimann, E. L., and Georgescu, M. M. (2006) *EMBO J.* **25,** 910–920
44. Vazquez, F., Matsuoka, S., Sellers, W. R., Yanagida, T., Ueda, M., and Devreotes, P. N. (2006) *Proc. Natl. Acad. Sci. U. S. A.* **103,** 3633–3638
45. Koradi, R., Billeter, M., and Wuthrich, K. (1996) *J. Mol. Graph.* **14,** 51–55
46. Kraulis, P. L. (1991) *J. Appl. Crystallogr.* **24,** 946–950
47. Nicholls, A. (1992) *GRASP: Graphical Representation and Analysis of Surface Properties*, Columbia University, New York
48. Laskowski, R. A., Rullmannn, J. A., MacArthur, M. W., Kaptein, R., and Thornton, J. M. (1996) *J. Biomol. NMR* **8,** 477–486